Using Polymer Conformation to Control Architecture in Semiconducting Polymer/Viral Capsid Assemblies

Benny C. Ng,[†,‡] Stephanie T. Chan,[†] Jason Lin,[†] and Sarah H. Tolbert[†,‡,*]

[†]Department of Chemistry and Biochemistry, UCLA, Los Angeles, California 90095-1569, United States, and [‡]California NanoSystems Institute, UCLA, Los Angeles, California 90095-7227, United States

ABSTRACT Cowpea chlorotic mottle virus is a single-stranded RNA plant virus with a diameter of 28 nm. The proteins comprising the capsid of this virus can be purified and reassembled either by themselves to form hollow structures or with polyanions such as double-stranded DNA or single-stranded RNA. Depending on pH and ionic strength, a diverse range of structures and shapes can form. The work presented here focuses on using these proteins to encapsulate a fluorescent polyanionic semiconducting polymer, MPS-PPV (poly-2-methoxy-5-propyloxy sulfonate phenylene vinlyene), in order to obtain optically active virus-like particles. After encapsulation, fluorescence from MPS-PPV shows two distinct peaks, which suggests the polymer may be in two conformations. A combination of TEM, fluorescence anisotropy, and sucrose gradient separation indicate that the blue peak arises from polymer encapsulated into spherical particles, while the redder peak corresponds to polymers contained in rod-like cages. Ionic strength during assembly can be used to tune the propensity to form rods or spheres. The results illustrate the synergy of hybrid synthetic/biological systems: polymer conformation drives the structure of this composite material, which in turn modifies the polymer optical properties. This synergy could be useful for the future development of synthetic/biological hybrid materials with designated functionality.

KEYWORDS: poly(2-methoxy-5-propyloxy sulfonate phenylene vinylene) · MPS-PPV · cowpea chlorotic mottle virus · CCMV · fluorescence anisotropy · self-assembly · virus-like particles

Over the past decade, the use of viruses has increased greatly in both biological and nonbiological research due to their versatility and wide ranging potential applications in materials science.[1] Efforts have been made to assess the range of materials that can be packaged inside a viral capsid and to determine if any physical limits exist on packaging. Cylindrical viruses such as tobacco mosaic virus (TMV) and M13 bacteriophage appear to have potential in the synthesis of nanowires,[2−4] in binding to metal surfaces using alterations in the capsid protein,[5−7] and in forming complex nanoscale architectures.[8] Spherical viruses, by contrast, have been used for a wide range of experiments mostly focusing on encapsulation of non-native materials. Previous studies have shown that spherical viruses such as brome mosaic virus (BMV) and cowpea chlorotic mottle virus (CCMV), which are composed of a single protein subunit, are able to form new bionanocomposites with many different nonbiological cores such as gold nanoparticles,[9−14] magnetic nanoparticles,[15] transition metal ions,[16,17] emulsion droplets,[18] and polymers.[19−22] In all of these examples, the virus cage remained in the native spherical structure; while the cargo was observed to modify the size of the sphere, it did not change the basic nanoscale architecture.

Unlike many other viruses, CCMV has the ability to form both spherical and rod-like structures. It is an icosahedral virus with 180 identical capsid proteins, which can easily assemble into a 28 nm capsid with a 15 to 18 nm empty core space depending on the ionic strength and pH of the solvent.[23] However, CCMV has shown a possibility of self-assembling into a non-native rod-like structure by varying the buffer environment or using double-strand DNA as a template.[23,24] The results suggest a new question, which is, how does the structure of the cargo affect the final structure of a viral nanocomposite in cases where nonspherical structures are possible? To begin to address this question, here we describe the coassembly of viral capsids with a luminescent semiconducting polymer as a route to both spherical and rod-like optically active bionanocomposites. The viral capsid is filled with the optically active semiconducting polymer, which in turn directs the assembly process through ionic strength mediated changes in polymer conformation.

Charged conjugated polymers have potential applications as both biological and chemical sensors,[25−28] cationic binders,[29]

* Address correspondence to tolbert@chem.ucla.edu.

Received for review August 11, 2010 and accepted September 24, 2011.

Published online September 25, 2011
10.1021/nn202493w

and electroluminescent material.[30,31] Conjugated polymers with neutral side chains are normally only soluble in organic solvents such as toluene, chloroform, and chlorobenzene because of their highly hydrophobic π-conjugated backbones. However, conjugated polymers can become water-soluble by attaching charged or neutral hydrophilic side chains such as ammonium salts,[32] carboxylates,[33] and ethylene glycol[34] to the hydrophobic backbones. Because the side chain solubility may be quite different from the backbone solubility, polymer−solvent interactions can also play an important role in determining the solution phase chain conformation of conjugated polymers such as poly(phenylene vinylenes),[35,36] polythiophenes,[37] and polyfluorenes.[38]

Because bends or kinks in the polymer break the π-conjugation, chain conformation also affects the luminescent properties For example, when poly-[2,5-bis(diethylaminetetraethylene glycol)phenylene vinylene] (a polar but nonionic PPV) is dissolved in chloroform, its hydrodynamics radius is 9.9 nm and it shows a 34% photoluminescence quantum yield. However, when this PPV derivative is dissolved in water, the strong hydrophobic interactions along the polymer backbone cause the polymer chain to collapse. Thus, its hydrodynamics radius and photoluminescence quantum yield in water decrease to 5.4 nm and 12%, respectively.[39] Since the polymer is π-conjugated, it can be thought of as a series of linked chromophores in good electronic contact.[40] The decrease in quantum yield is generally attributed to the formation of nonradiative trap and kink sites that can harvest excitations form the entire linked polymer. Quantum yield decreases are usually accompanied by shifts in both absorption and emission: highly coiled polymers have shorter conjugated segments compared to more elongated polymers, resulting in blue-shifts. When the solubility is low enough, however, coiling is accompanied by aggregation, which often results in red-shifted emission because of the formation of interchain excited states and the potential for rapid energy transfer between aggregated segments to find low-energy emissive states. This type of behavior is general to a broad range of conjugated polymers, all of which aggregate in poor solvents. For instance, a dioctyl-substituted polyfluorene (PFO) in the very poor solvent cyclohexane shows a red-shifted aggregate absorption peak.[38] By contrast, poly(3-dodecylthiophene) (P3DDT) chains have a more extended structure and redder emission in the good solvent chloroform compared to the moderate solvent THF.[37]

For charged semiconducting polymers, one of the easiest ways to tune this solubility is using ionic strength. As the ionic strength of an aqueous solutions increases, counterion condensation occurs, which decreases solubility and causes increased polymer coiling and aggregation. For example, dynamic light scattering (DLS) measurements of (poly-2-methoxy-5-propyloxy sulfonate phenylene vinlyene) [MPS-PPV][25] indicate that that the hydrodynamic diameter decreases from 93 to 44 nm when just 1 mM LiCl is added to neat water.[41]

For virus encapsulation studies, MPS-PPV and related polyanionic semiconducting polymers have a number of advantages. Unlike previous studies on encapsulation of nonfluorescent polymers such as polystyrene sulfonate[21] (PSS) and polyanetholesulphonic acid[22] by CCMV, MPS-PPV is a conjugated polymer that absorbs and emits strongly in the visible light region. As discussed above, the chain conformation and thus the luminescent properties are highly sensitive to solvent and ionic strength, creating a viral guest molecule that can be manipulated using solution conditions and can report back optically on it conformation. For example, when MPS-PPV is in a polar aprotic solvent such as DMSO, the polymer chain is stretched out because DMSO is a reasonable solvent for both the polar side chains and the nonpolar backbone. In water, only the ionic side chains of MPS-PPV confer solubility, and so the polymer tends to coil in an effort to hide the hydrophobic core. Consequently, the photoluminescence quantum yield of MPS-PPV in DMSO is nearly 100 times greater than that in water.[41] Similar to the negatively charged RNA, MPS-PPV is polyanionic, which facilitates the encapsulation process with the capsid proteins. Other advantages include its commercial availability and its water solubility. Finally the conjugated nature of these polymers both makes them luminescent and makes them sit on the rod−coil boundary. This dynamic structural heterogeneity makes MPS-PPV an interesting system to explore the effect of cargo solvation on the geometry of the final viral composite.

In this work, we combine all of these ideas to explore how dynamic solution phase structural variation can affect viral packaging. The ionic strength of the solvent is used to control polymer conformation, which, in turn, controls virus cage structure. Fluorescence spectroscopy and fluorescence anisotropy measurements are utilized to explore changes in the local polymer conformation and environment and the nature of its association with viral capsids. Transmission electron microscopy (TEM) is used for structural characterization of the capsids/polymer composite. We find that viruses do not simply form spherical structures, as they do when encapsulating flexible polymers such as PSS. Instead, the polymer's stretched or coiled state acts as a template to alter the structure of the virus-like particles (VLPs) assembled.

RESULTS AND DISCUSSION

Our overall strategy was to coassemble purified capsid proteins with MPS-PPV to produce an optically active bionanocomposite. To control polymer conformation in solution, this was performed at different ionic strengths. Specifically, initial sodium chloride concentrations of 0.0, 0.1, and 1.0 M were used, followed by dialysis against a moderate ionic strength solution termed RNA assembly buffer to bring all

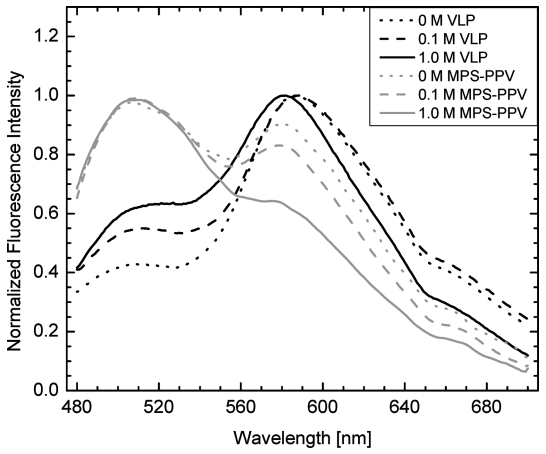

Figure 1. Comparison of normalized fluorescence spectra of pure MPS-PPV and MPS-PPV-based virus-like particles (VLPs) assembled using different initial ionic strengths. The 510 nm peak corresponds to the fluorescence from highly coiled MPS-PPV, while the 590 nm peak corresponds to the fluorescence from MPS-PPV with a more elongated conformation. For both the pure MPS-PPV and the VLP samples, the relative intensity of the 510 nm peak grows as a function of initial ionic strength, indicating an increasing amount of highly coiled chains at higher ionic strength. Note that to prevent spectral overlap, the pure MPS-PPV samples are normalized to the 510 nm peak, while the VLP samples are normalized to the peak at 590 nm.

samples to the same final solution conditions. A ratio of 180 capsid proteins to 1 polymer was used to mimic 180 capsid proteins per RNA in wild-type CCMV.

After each sample was prepared, steady-state fluorescence experiments were performed. Figure 1 compares normalized emission spectra of MPS-PPV only and VLPs in the RNA assembly buffer. The samples differ only in the initial concentration of sodium chloride used during assembly. Each sample exhibits two distinct peaks around 510 and 590 nm. While the peak around 655 nm has been shown to be a vibronic subband of the 590 nm peak, the other two peaks do not share this relationship.[42] The energy difference between the 510 nm peak and the peak at 590 nm is 0.33 eV, which is larger than the 0.21 eV vibrational spacing observed for PPV-based polymers. Below, we will also use fluorescence anisotropy data to further support the idea that the peaks at 510 and 590 nm are not vibronic sub-bands.

The presence of two distinct luminescence bands suggests that the polymer is in two different conformations in our virus-like particles. As mentioned earlier, the coil size and fluorescence quantum yield of MPS-PPV decreases with increasing ionic strength. When the sodium chloride concentration changes from 0.0 to 1.0 M in Figure 1, the fluorescence peak for both the pure polymer and VLP samples exhibits a blue-shift, which indicates that the polymer coils more tightly in 1.0 M NaCl than in 0.0 M NaCl solutions. When the polymer coils, its conjugation length decreases and the emission moves to shorter wavelength. Conversely, the polymer emits at a longer wavelength when the chains are more elongated and the polymer has a longer conjugation length. Thus, the presence of two distinct luminescence peaks in our virus-like particles suggests that both coiled and more elongated polymer chains can coassemble with the virus capsid protein.

If the idea that virus-like particles can form with either stretched or coiled polymer chains is correct, then the relative intensity of the two peaks should change depending on its initial ionic strength. We find that this is indeed the case (Figure 1). As the ionic strength increases, the relative intensity of the coiled (510 nm) peak increases. The ratio between the two peaks provides some measure of the relative amount of the two structures and how that ratio can be tuned by varying ionic strength. We note that the normalized spectra of pure MPS-PPV samples have their highest peak at 510 nm, indicating an overall more coiled conformation for polymer without a viral shell. This is because this fairly hydrophobic polymer coils tightly in the buffer, which leads to a shorter conjugation length and also a lower quantum yield. Indeed, when the luminescence data are not normalized, one finds that the polymer-only samples fluoresce much less than the encapsulated polymer samples (data not shown). Again, however, the relative intensity of the coiled (510 nm) peak in the pure polymer increases with increasing ionic strength, as it does in the VLPs. Together, these results indicate that formation of the polymer/protein nanostructure in general and the formation of elongated polymer chains in particular help reduce nonradiative relaxation processes that lead to luminescence quenching.

We note that the correlation between polymer conformation and luminescence quantum efficiency means that it is not possible to directly read the relative population of coiled and elongated polymer from the graph in Figure 1. It is well established that PPV-based polymers show a higher quantum yield for straight chains than coiled chains because kinks in the polymer chain cause defects that can self-quench luminescence.[43−47] The exact quantum yield varies with the details of the structure, however. What we can say is that the relative luminescence efficiency for straight chains is always higher than for coiled chains, and so the fact that the 590 nm peak in Figure 1 is always greater than the 510 nm peak for the VLPs does not mean that all samples contain predominantly elongated structures. It does mean that all VLP samples contain some elongated structures, though the fraction could be quite small if the quantum efficiency is high enough.

Thus, while luminescence measurements are an excellent way to probe local polymer structure and relative changes in population, they do not provide information about absolute populations because of quantum efficiency changes, and they only suggest the shape of the VLP. Because of this, we turn to transmission

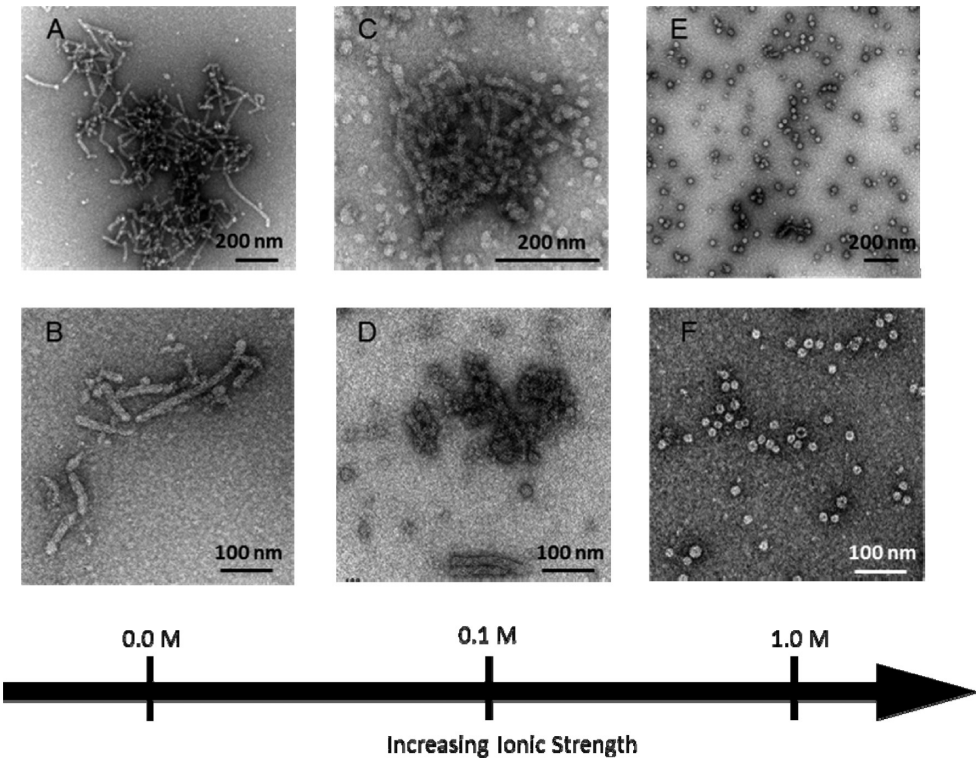

Figure 2. TEM images of MPS-PPV/CCMV virus-like particles assembled at various ionic strengths. (A, B) Materials assembled at 0.0 M NaCl. These images show mostly rod-like structures of various lengths. (C, D) Materials generated with an initial NaCl concentration of 0.1 M. These images show a mixture of rod-like and spherical structures; the rod-like structures are shorter in length compared to structures assembled with 0.0 M NaCl. (E, F) Materials assembled with an initial NaCl concentration of 1.0 M display mostly spherical structures. These spherical virus-like particles are similar to the ones formed by encapsulation of polystyrene sulfonate (PSS) (Figure 3B).

electron microscopy to image the actual structure being formed as a function of ionic strength (Figure 2). As seen in panels E and F of Figure 2, for virus-like particles assembled with 1.0 M NaCl, mostly spherical structures between 22 and 26 nm were observed. At that high ionic strength, the polymer apparently coils so tightly that spherical structures are the dominant assembly motif. By contrast, as we lower the ionic strength to 0.0 M NaCl, we found mostly rod-like structures ranging from 100 to 1000 nm in length with very few spherical structures (Figure 2A and B). At this low ionic strength, the MPS-PPV apparently does not coil so tightly and so the capsid protein can encapsulate the stretched polymer and form a rod-like structure.

Although the polymer is not monodisperse, the length variation in VLP is unlikely to come entirely come from the polydispersity of the MPS-PPV. While determining the size of conjugated polyelectrolytes is notoriously difficult, for this sample the polymer was dialyzed against a 50 kDa membrane during purification to eliminate chains smaller than 50 kDa. Given the nature of the synthetic methods used to produce the polymer, it is likely that most of the polymer is less than 100 kDa.[41] This 2× size range is much smaller than the order of magnitude length variations observed in Figure 2, and thus it is likely that the longest structures contain many polymer chains and the variation is a result of the dynamic fluctuations that occur during the assembly process.

At intermediate ionic strength (0.1 M NaCl), we observed a mixture of rod-like and spherical structures (Figure 2C and D). The rod-like structures are generally shorter than the ones formed at 0.0 M NaCl because the polymer chains are less open at 0.1 M NaCl. The spherical structures are around 24−28 nm, slightly larger than the ones formed at 1.0 M NaCl. As mentioned earlier, the coil size of MPS-PPV in solution decreases with increasing ionic strength. The observation of larger VLPs at lower ionic strength is completely consistent with this established behavior.

Figure 3 displays the TEM images of both negative and positive control samples. In the absence of MPS-PPV, the capsid proteins lack of any specific structure or shape under all three assembly conditions (Figure 3A) because the proteins do not have a structure-directing template and aggregate together through nonspecific protein−protein interactions under the conditions used in this work. On the basis of this control, we can conclude that all of the spherical and rod-like shapes in Figure 2 must contain MPS-PPV. To ensure the quality of the capsid proteins and the ability to form spherical capsids under these conditions, poly(styrene sulfonate) was chosen as a control template. This polyanionic polymer has been demonstrated to form spherical virus-like

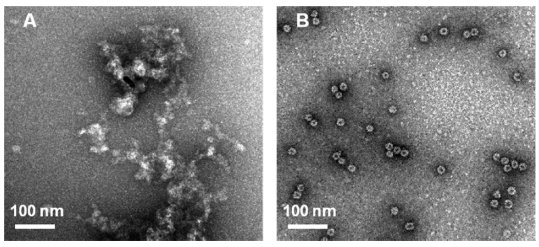

Figure 3. TEM images of various control samples. (A) Capsid proteins only without any polymer. This image shows that protein that is not associated with an anionic polymer aggregates with no specific structure under the conditions used in this work. Similar random aggregates are formed at all the ionic strengths used in this work. (B) The capsid protein can encapsulate PSS to form VLPs under the full range of ionic strengths used in this work. This control shows that the effect of ionic strength on capsid assembly itself is not responsible for the structural variation shown in Figure 2.

particles in the past (Figure 3B).[21] Indeed, as a thorough control, we have shown that PSS can be packaged inside a viral capsid to form exclusively spherical particles like those shown in Figure 3B under all three assembly conditions employed in this work (data not shown). Unlike MPS-PPV, PSS does not have a conjugated backbone, and thus it is a more flexible polymer that tends to form fairly tight coils at all ionic strengths. This leads to spherical virus-like particles under all conditions. This control thus allows us to conclude that it is not the effect of ionic strength on the capsid protein that produces the structural variation shown in Figure 2, but instead the ionic strength induced changes in the MPS-PPV structure.

Comparison of Figures 2 and 3 indicates that a rigid polymer like MPS-PPV can direct the capsid protein to form a non-native structure (*i.e.*, a rod rather than a sphere). This result is in agreement with studies where double-stranded DNA was used as a structure-directing agent and rod-like structures were also formed.[24] The results from TEM are also consistent with the previously discussed fluorescence data in Figure 1. From the TEM images, the formation of spherical structures increased as a function of increasing ionic strength, which corresponded to the relative increase in peak height at 510 nm in the fluorescent experiment. The TEM data supports the conclusions drawn from the fluorescence study that the peaks at 510 and 590 nm correspond to spherical and rod-like structures, respectively. The low population of rods in images collected on samples produced at 1.0 M NaCl also confirms our hypothesis that the luminescence quantum yield is much higher for rod-like VLPs than for spherical VLPs.

To further confirm the relationship between the conformation of the encapsulated MPS-PPV and the physical structure of the protein/polymer assembly, fluorescence anisotropy was measured for each of the three samples discussed above. Fluorescence anisotropy is a measurement of the difference in the emission intensity with polarization parallel and perpendicular to the polarization of the exciting light divided by the total intensity. Because it is a ratio, the anisotropy value is independent of the total intensity and the concentration of the fluorophore.[48] For an unaligned sample in the absence of any dynamic processes, the anisotropy quantifies the difference (in degrees) between the excitation transition dipole and the emission dipole according to[48]

$$r_o = \frac{2}{5}\left(\frac{3\cos^2\beta - 1}{2}\right) \quad (1)$$

where r_o is the anisotropy observed in the absence of other depolarizing processes and β is the angle between the two primary absorption and emission axes. Fast dynamic processes, such as rapid molecular motion or excited-state energy transfer, can scramble the polarization, however, resulting in a reduced anisotropy value. While physical motion is not likely to have a major effect, given the large size of the virus-like particles studied here, Förester energy transfer between chromophores in aggregated semiconducting polymers has been shown to be quite fast and can completely scramble polarization.[49] According to eq 1, the anisotropy value varies between 0.4 to −0.2 as the emission polarization varies from 0° to 90° with respect to the excitation polarization. For a randomly oriented sample with parallel absorption and emission dipoles, the anisotropy would be 0.4 in the absence of any dynamic process, but would decrease toward zero if dynamic processes change the physical orientation of the excited chromophore on the time scale of the emission lifetime.[50]

Fluorescence anisotropy can thus provide insight about conformation in semiconducting polymers. When the polymer is coiled up, a population of excited molecules with the same polarization can undergo many random hops between sites with different orientations of the transition dipoles *via* intra- or interchain Förster transfer. This scrambles the overall polarization of the excited-state population, causing a low fluorescence anisotropy value for the coiled polymer.[50] If the chains are straight and parallel to each other within each aggregate, Förster hopping might still occur, but it does not result in a scrambling of the polarization memory because all of the transition dipoles in the aggregate are parallel. As a result, an anisotropy value near 0.4 is expected for either isolated, uncoiled semiconducting polymers or polymers that are aggregated, but where the chains are straight and parallel to each other.[49]

Figure 4 shows the measured fluorescence anisotropy for MPS-PPV in various configurations. We note that these values are obtained by taking the difference between two low-concentration and thus fairly noisy luminescence spectra. By comparing results from nominally identical samples, we estimate a statistical error of 18% in these anisotropy values. This error must be considered when interpreting the data. The anisotropy for all the virus-like particles shows basically the same trend. In the blue region around 500 nm, the anisotropy

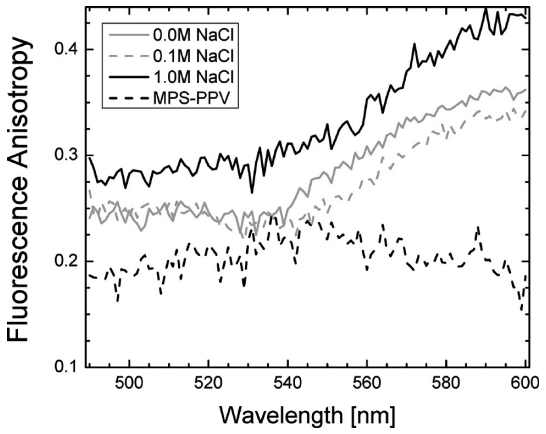

Figure 4. Comparison of fluorescence anisotropy for pure MPS-PPV and for MPS-PPV/CCMV virus-like particles. The low anisotropy value observed for the neat polymer solution over the range of wavelengths shown here indicates a coiled polymer structure that loses polarization memory through energy transfer. By contrast, the virus-like particles show two distinct anisotropy values and a transition between them. The low anisotropy value around 510 nm suggests that this luminescence arises from polymer in a coiled configuration (spherical structures) similar to the pure MPS-PPV in solution. The high anisotropy value around 590 nm indicates that this luminescence arises from polymer in a stretched conformation (rod-like structures) because it can retain its excited-state polarization memory. Comparison of multiple runs on nominally identical samples gives an error of ~18% for all anisotropy values.

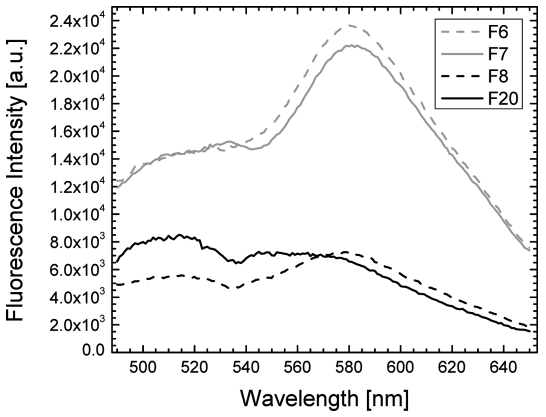

Figure 5. Luminescence from MPS-PPV/CCMV virus-like particles separated by centrifugation through a continuous linear sucrose gradient; all fractions (F) showing significant MPS-PPV luminescence are shown. Fractions 6 and 7 show a dominance of the 590 nm peak, while in fraction 20, the 510 nm peak is more obvious. This suggests that the spherical structures move much faster through the gradient as compared to the rod-like structures because the spherical structures are located at lower fractions in the gradient. More importantly, the data show that the different structures shown in Figure 2 can be physically separated, creating populations with more homogeneous optical properties.

is fairly low. The value then increases toward the red, reaching a value very near 0.4 at 590 nm. The anisotropy variation around 500 nm among three different VLP samples is not statistically significant, but the variation between the 500 and 590 nm is statistically significant. By contrast, the unencapsulated MPS-PPV sample shows a relative low anisotropy of 0.2, which is constant across all wavelengths.

Since the unencapsulated MPS-PPV coils fairly tightly in the buffer, its anisotropy value should be the lowest among all samples because polarized excitons can undergo many intra- and interchain transfers that result in a loss of polarization memory. For the encapsulated MPS-PPV, the spherical structures should also have a smaller anisotropy value because the coiled MPS-PPV conformation allows for scrambling of excited-state polarization memory through inter- and intrachain Förster transfers. By contrast, the rod-like structures should show a greater anisotropy value because polymer chains are straight and parallel and Förster transfer between segments can occur without scrambling the polarization. For the encapsulated MPS-PPV samples, the plateau around ~0.27 between 480 and 540 nm thus corresponds to a coiled structure. There is a transitional region between 530 and 580 nm, and then the anisotropy eventually plateaus again at 590 nm with a value of 0.4, corresponding to extended chains.

While it is reassuring that the anisotropy data lead to the same conclusions drawn from luminescence peak shifts and from TEM imaging, the data also confirm our supposition that the 510 and 590 nm luminescence peaks correspond to different physical structures, rather than to vibronic structure within a single luminescence band. If the peaks at 510 and 590 nm came from vibronic structure, one would expect their anisotropy values to be the same. Capsid protein can thus use MPS-PPV as a template to form different structures depending on the ionic strength and that these structures exhibit different fluorescence properties.

To further test our hypothesis that two physically different structures with differed optical properties could be produced, separation of the two structures was attempted. If each structure contains only one physical conformation of MPS-PPV, we should be able to separate the two fluorescent species using continuous linear sucrose gradient centrifugation. Here a sucrose gradient is produced and separation occurs based on both density matching and diffusion time through the gradient. After separation, the tube is divided into fractions, which are probed for the presence of virus-like particles using fluorescence intensity. Figure 5 shows data for a sample made with 0.0 M NaCl, which we expect to contain mostly rods and a few spheres. Fractions 6–8 and 20 showed MPS-PPV luminescence of reasonable intensity. The spectra were not all the same, however. The upper three bands of the gradient showed a much more intense peak at 590 nm than at 510 nm, suggesting that the rod-like structure travels more slowly in the gradient as compared to the spherical structure because of the larger hydrodynamic radius (Strokes radius) and moment of inertia. On the other hand, the bottom fraction (20) contains a peak at 510 nm without a peak at 590 nm.

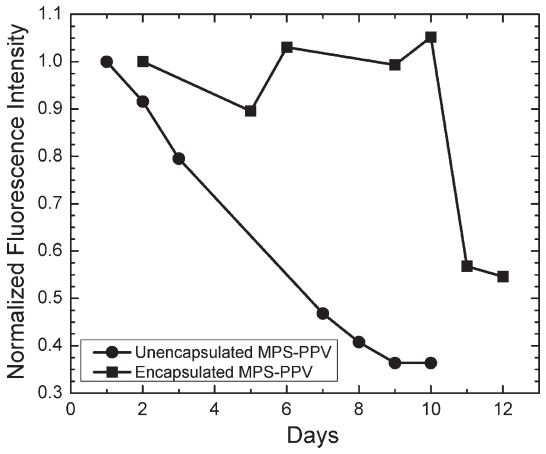

Figure 6. Comparison of normalized fluorescence intensity at 590 nm for the encapsulated MPS-PPV (■) assembled at 1.0 M NaCl and unencapsulated MPS-PPV (●) over a 12-day period. The encapsulated MPS-PPV retains its fluorescence intensity with little change until day 10. However, the unencapsulated MPS-PPV shows a gradual decrease in fluorescence intensity over a 10-day period. The comparison indicates that encapsulated MPS-PPV is more stable toward oxidation than unencapsulated MPS-PPV.

The ability to physically separate our samples helps confirm the idea of two unique structures that can be tuned using ionic strength.

A final experiment also shows that the virus-like particles show luminescence that is more stable under ambient conditions than that observed in the unencapulated polymer. Figure 6 compares the normalized fluorescence at 590 nm for polymer encapsulated at 1.0 M NaCl and unencapsulated polymer over a 12-day period. The data are normalized to the intensity at 590 nm on the first day to compare the relative intensity during each day for the two samples. The unencapsulated polymer shows a gradual decrease in intensity, while the encapsulated polymer retains its fluorescence intensity until day 10, when the intensity drops significantly. This data demonstrates that the virus-like particles, particularly those with an elongated structure, which dominate the luminescence at 590 nm, are more oxidatively stable than pure polymer. This is likely because the kinks in the polymers that quench luminescence also provide a site for oxidative damage. Thus rod-like VLPs in specific impart both biological compatibility and enhanced quantum yield and lifetime.

CONCLUSIONS

In this work, we explored the process of encapsulating a foreign substance into a protein cage using MPS-PPV contained in CCMV capsids as a model system. We have shown that we are able to create two distinct, optically active structures by coassembling MPS-PPV with purified CCMV capsid protein at different ionic strengths. At high ionic strength, the polymer tends to coil in solution, and so it templates the formation of spherical virus-like particles with dimensions that are very similar to the native structure. At low ionic strength, however, this semirigid rod polymer adopts a more extended conformation, and so it drives the formation of rod-like structures. A combination of TEM and fluorescence anisotropy confirms that the spheres contained coiled polymer while the rod-like structure contains stretched polymer. Sucrose gradient studies further show that two populations can be separated.

This work was enabled by the flexibility of both the polymer and the capsid protein. MPS-PPV shows a broad range of conformations in aqueous solutions, depending on ionic strength. The CCMV capsid protein is also unique in that it is able to conform to the shape of its molecular cargo and is not limited to its native spherical structure. The fact that MPS-PPV is an organic semiconductor with optical properties that are highly sensitive to polymer conformation further provides a unique opportunity to probe both the overall geometry of these synthetic virus-like particles and the detailed conformation of the cargo. While this work focuses only on MPS-PPV, the key conclusions should be general to the broad range of polycharged species that can be used to nucleate capside formation.

In considering the impact of this work, it is interesting to consider how this study complements what is currently known about viral packaging of non-native materials. It is now well established that CCMV and other related viral proteins can package non-native material, including species with both globular and elongated structures. What this work adds is an understanding that when a fluctuating population is packaged, the final structures formed appear to contain a static snapshot of the dynamically inhomogeneous population. That in turn indicates that a range potentially interesting nonequilibrium structures may be formed as synthetic/viral conjugates, and even if those structures are not the dominant conformation, they may be separable from the larger population. As such, this work opens the door to creating more diverse virus-based materials by taking advantage of the inhomogeneity always present in self-assembling systems.

METHODS

Inoculum, Infection, and Leaf Harvest. Modifying Jean-Philippe's procedure,[51] the infected cowpea plants (cowpea California black eye no. 5) were infected with CCMV by blending 15 g of previously infected cowpea leaves in homogenization buffer (0.2 M sodium acetate at pH 4.8 and 0.01 M disodium EDTA) with 3% (w/v) carborundum powder, which helps break through the plant cell walls when the inoculum is applied. This mixture was

rubbed on the cowpea plant's primary leaves. After a few days, symptoms of infection including a dark red ring around the stem and brownish yellow spots on the leaves appeared. The leaves were harvested and stored at −80 °C.

Virus Purification. The virus purification was performed at 4 °C using ultrafiltration,[51] which was modified from Bancroft's early work.[23] Approximately 100 g of frozen infected leaves was homogenized in an equal volume of homogenization buffer. The homogenate was pressed through two layers of cheesecloth placed diagonally on top of each other to remove the leaf tissue. The filtered homogenate was centrifuged for 15 min at 10 000 rpm using the RC-5 Superspeed Refrigerated Centrifuge, and the supernatant was collected, discarding the pellet. Then, 10% (w/v) PEG-8000 (polyethylene glycol) was added and stirred overnight. The solution was centrifuged for 10 min at 10 000 rpm, and the pellet was resuspended in virus buffer (0.1 M sodium acetate at pH 4.8). Following centrifugation for 10 min at 10 000 rpm to remove the impurities, 15% (w/v) PEG-8000 was added to the supernatant and left to stir overnight. The solution was centrifuged for 10 min at 10 000 rpm. The pellet was resuspended in the virus buffer and was centrifuged again for 10 min at 10 000 rpm to collect the supernatant. The purified viruses were concentrated in a Biomax-100,000 centricon and stored at −80 °C until use. UV−vis spectroscopy was used to determine the purity of the viruses by dividing the absorbance at 260 nm by the absorbance at 280 nm; an Abs_{260}/Abs_{280} ratio of 1.5 to 1.7 is normal for CCMV.[51] The concentration (mg/mL) of the viruses was calculated by using the conversion $OD_{260} = 1$ in a 1 cm cuvette path length corresponds to 0.17 mg/mL protein.[51] An average yield of 20 mg of CCMV per 100 g of leaves was obtained.

Capsid Protein Purification. The CCMV capsid protein purification was developed by Choi and Rao.[52] Purified viruses were dialyzed overnight in disassembly buffer containing 500 mM calcium chloride, 50 mM Tris-HCl at pH 7.5, 1 mM EDTA, 1 mM DTT, and 0.5 mM PMSF. The dialysate was centrifuged at 14 000 rpm for 30 min, and the precipitated RNA was discarded. The supernatant was dialyzed in RNA assembly buffer (50 mM sodium chloride, 50 mM Tris-HCl at pH 7.2, 10 mM potassium chloride, 5 mM magnesium chloride, and 1 mM DTT). This buffer gave the optimal conditions to allow any residual RNA in the supernatant to assemble into viruses again. Following dialysis, the sample was centrifuged for 100 min at 100 000 rpm to pellet any reassembled viruses. The supernatant contained pure capsid proteins. UV−vis absoprtion was used to determine the concentration of the proteins.

Encapsulation of MPS-PPV. The freshly prepared purified capsid proteins were dialyzed overnight in storage buffer (20 mM Tris-HCl pH 7.2, 1 mM EDTA, 1 mM DTT, and 1 mM PMSF) under three different sodium chloride concentrations of 0.0, 0.1, and 1.0 M. The salt concentrations and pH can change how the capsid proteins form its structure.[23,24] Finally, MPS-PPV with an estimated molecular weight between 50 and 100 kDa was added at a ratio of 180 capsid proteins to one polymer and dialyzed in RNA assembly buffer overnight in the dark. The total volume for each sample was adjusted to 0.7 mL by addition of storage buffer, and the final polymer concentration was 100 nM in all samples.

TEM Preparation. Copper grids (Ted Pella, Redding, CA) of 400 meshes were coated with Parlodion and carbon. A drop of the sample (10 μL) was placed onto the copper grid and incubated for 1 min. The excess solution was then removed by lightly blotting the grid on a Whatman 4 filter paper, following which the sample was negatively stained with 1% uranyl acetate and air-dried. The TEM samples were imaged with a JEM1200-EX electron microscope at an accelerating voltage of 80 kV.

Fluorescence Spectroscopy and Anisotropy. Fluorescence spectra of MPS-PPV-containing samples were collected using a JY-Horiba Fluorolog-3. A 0.15 mL aliquot of each encapsulated MPS-PPV sample was excited at 450 nm and scanned from 470 to 700 nm with an integration time of 15 s. The spectra were obtained by dividing the emission intensity by the lamp intensity and then were corrected by subtracting the fluorescence spectrum of the pure buffer under the same conditions. Fluorescence anisotropy was collected on the same fluorimeter with the addition of excitation and emission polarizers at either a vertical or a horizontal orientation. To calculate anisotropy, we first corrected the emission at each wavelength by dividing it with the light intensity of the fluorimeter. Then, the corrected intensity of the four orientations with eq 1 was used to solve for the anisotropy at each wavelength.

Continuous Linear Sucrose Gradient Centrifugation. The sucrose gradient was prepared by freezing a 25% (w/v) sucrose solution for one hour in a −80 °C freezer, then letting it thaw overnight. One milliliter of the sample was slowly loaded on top of the gradient and centrifuged for 30 min at 40 000 rpm using a SW-41 rotor. After centrifugation, the sucrose gradient was fractionated into 20 tubes; fluorescence from each fraction was then measured.

Acknowledgment. This work was supported by the National Science Foundation through a Collaborative Research in Chemistry Grant (CHE-0527015), through an IGERT Grant (DGE-0114443), and through instrumentation Grant DMR-0114002. Additional support came from an NIH Initiative for Maximizing Student Diversity Grant, the University of California Leadership Excellence through Advanced Degrees program (UC LEADS), the UCLA Undergraduate Research Fellow Program (URFP), and the California NanoSystems Institute (CNSI). We thank A. D. Smith for synthesizing the MPS-PPV used in this work and M. L. Philips for help preparing TEM grids.

REFERENCES AND NOTES

1. Flynn, C. E.; Lee, S. W.; Peelle, B. R.; Belcher, A. M. Viruses as Vehicles for Growth, Organization and Assembly of Materials. *Acta Mater.* **2003**, *51*, 5867–5880.
2. Nam, K. T.; Kim, D. W.; Yoo, P. J.; Chiang, C. Y.; Meethong, N.; Hammond, P. T.; Chiang, Y. M.; Belcher, A. M. Virus-Enabled Synthesis and Assembly of Nanowires for Lithium Ion Battery Electrodes. *Science* **2006**, *312*, 885–888.
3. Nam, K. T.; Lee, Y. J.; Krauland, E. M.; Kottmann, S. T.; Belcher, A. M. Peptide-Mediated Reduction of Silver Ions on Engineered Biological Scaffolds. *ACS Nano* **2008**, *2*, 1480–1486.
4. Niu, Z.; Liu, J.; Lee, L. A.; Bruckman, M. A.; Zhao, D.; Koley, G.; Wang, Q. Biological Templated Synthesis of Water-Soluble Conductive Polymeric Nanowires. *Nano Lett.* **2007**, *7*, 3729–3733.
5. Basu, G.; Allen, M.; Willits, D.; Young, M.; Douglas, T. Metal Binding to Cowpea Chlorotic Mottle Virus Using Terbium-(III) Fluorescence. *J. Biol. Inorg. Chem.* **2003**, *8*, 721–725.
6. Lee, S. W.; Mao, C. B.; Flynn, C. E.; Belcher, A. M. Ordering of Quantum Dots Using Genetically Engineered Viruses. *Science* **2002**, *296*, 892–895.
7. Miller, R. A.; Presley, A. D.; Francis, M. B. Self-Assembling Light-Harvesting Systems from Synthetically Modified Tobacco Mosaic Virus Coat Proteins. *J. Am. Chem. Soc.* **2007**, *129*, 3104–3109.
8. Huang, Y.; Chiang, C. Y.; Lee, S. K.; Gao, Y.; Hu, E. L.; De Yoreo, J.; Belcher, A. M. Programmable Assembly of Nanoarchitectures Using Genetically Engineered Viruses. *Nano Lett.* **2005**, *5*, 1429–1434.
9. Slocik, J. M.; Naik, R. R.; Stone, M. O.; Wright, D. W. Viral Templates for Gold Nanoparticle Synthesis. *J. Mater. Chem.* **2004**, *15*, 749–753.
10. Chen, C.; Daniel, M. C.; Quinkert, Z. T.; De, M.; Stein, B.; Bowman, V. D.; Chipman, P. R.; Rotello, V. M.; Kao, C. C.; Dragnea, B. Nanoparticle-Templated Assembly of Viral Protein Cages. *Nano Lett.* **2006**, *6*, 611–615.
11. Dixit, S. K.; Goicochea, N. L.; Daniel, M. C.; Murali, A.; Bronstein, L.; De, M.; Stein, B.; Rotello, V. M.; Kao, C. C.; Dragnea, B. Quantum Dot Encapsulation in Viral Capsids. *Nano Lett.* **2006**, *6*, 1993–1999.
12. Dragnea, B.; Chen, C.; Kwak, E. S.; Stein, B.; Kao, C. C. Gold Nanoparticles as Spectroscopic Enhancers for *in Vitro* Studies on Single Viruses. *J. Am. Chem. Soc.* **2003**, *125*, 6374–6375.
13. Loo, L.; Guenther, R. H.; Basnayake, V. R.; Lommel, S. A.; Franzen, S. Controlled Encapsidation of Gold Nanoparticles by a Viral Protein Shell. *J. Am. Chem. Soc.* **2006**, *128*, 4502–4503.
14. Sun, J.; DuFort, C.; Daniel, M. C.; Murali, A.; Chen, C.; Gopinath, K.; Stein, B.; De, M.; Rotello, V. M.; Holzenburg,

A.; *et al*. Core-Controlled Polymorphism in Virus-Like Particles. *Proc. Natl. Acad. Sci. U. S. A.* **2007**, *104*, 1354–1359.
15. Huang, X. L.; Bronstein, L. M.; Retrum, J.; Dufort, C.; Tsvetkova, I.; Aniagyei, S.; Stein, B.; Stucky, G.; McKenna, B.; Remmes, N.; *et al*. Self-Assembled Virus-like Particles with Magnetic Cores. *Nano Lett.* **2007**, *7*, 2407–2416.
16. Hooker, J. M.; Datta, A.; Botta, M.; Raymond, K. N.; Francis, M. B. Magnetic Resonance Contrast Agents from Viral Capsid Shells: a Comparison of Exterior and Interior Cargo Strategies. *Nano Lett.* **2007**, *7*, 2207–2210.
17. Liepold, L.; Anderson, S.; Willits, D.; Oltrogge, L.; Frank, J. A.; Douglas, T.; Young, M. Viral Capsids as MRI Contrast Agents. *Magn. Reson. Med.* **2007**, *58*, 871–879.
18. Chang, C. B.; Knobler, C. M.; Gelbart, W. M.; Mason, T. G. Curvature Dependence of Viral Protein Structures on Encapsidated Nanoemulsion Droplets. *ACS Nano* **2008**, *2*, 281–286.
19. Raja, K. S.; Wang, Q.; Gonzalez, M. J.; Manchester, M.; Johnson, J. E.; Finn, M. G. Hybrid Virus-Polymer Materials. 1. Synthesis and Properties of PEG-Decorated Cowpea Mosaic Virus. *Biomacromolecules* **2003**, *4*, 472–476.
20. Ren, Y. P.; Wong, S. M.; Lim, L. Y. *In Vitro*-Reassembled Plant Virus-Like Particles for Loading of Polyacids. *J. Gen. Virol.* **2006**, *87*, 2749–2754.
21. Hu, Y. F.; Zandi, R.; Anavitarte, A.; Knobler, C. M.; Gelbart, W. M. Packaging of a Polymer by a Viral Capsid: The Interplay between Polymer Length and Capsid Size. *Biophys. J.* **2008**, *94*, 1428–1436.
22. Douglas, T.; Young, M. Host-Guest Encapsulation of Materials by Assembled Virus Protein Cages. *Nature* **1998**, *393*, 152–155.
23. Bancroft, J. B.; Hills, G. J.; Markham, R. A Study of Self-Assembly Process in a Small Spherical Virus-Formation of Organized Structures from Protein Subunits *In Vitro*. *Virology* **1967**, *31*, 354–379.
24. Mukherjee, S.; Pfeifer, C. M.; Johnson, J. M.; Liu, J.; Zlotnick, A. Redirecting the Coat Protein of a Spherical Virus to Assemble into Tubular Nanostructures. *J. Am. Chem. Soc.* **2006**, *128*, 2538–2539.
25. Chen, L. H.; McBranch, D. W.; Wang, H. L.; Helgeson, R.; Wudl, F.; Whitten, D. G. Highly Sensitive Biological and Chemical Sensors Based on Reversible Fluorescence Quenching in a Conjugated Polymer. *Proc. Natl. Acad. Sci. U. S. A.* **1999**, *96*, 12287–12292.
26. Dwight, S. J.; Gaylord, B. S.; Hong, J. W.; Bazan, G. C. Perturbation of Fluorescence by Nonspecific Interactions between Anionic Poly(phenylenevinylene)s and Proteins: Implications for Biosensors. *J. Am. Chem. Soc.* **2004**, *126*, 16850–16859.
27. Chemburu, S.; Ji, E.; Casana, Y.; Wu, Y.; Buranda, T.; Schanze, K. S.; Lopez, G. P.; Whitten, D. G. Conjugated Polyelectrolyte Supported Bead Based Assays for Phospholipase A2 Activity. *J. Phys. Chem. B* **2008**, *112*, 14492–14499.
28. Wang, D.; Gong, X.; Heeger, P. S.; Rininsland, F.; Bazan, G. C.; Heeger, A. J. Biosensors from Conjugated Polyelectrolyte Complexes. *Proc. Natl. Acad. Sci. U. S. A.* **2002**, *99*, 49–53.
29. Wang, H. L.; McBranch, D. W.; Donohoe, R. J.; Xu, S.; Kraabel, B.; Chen, L. H.; Whitten, D.; Helgeson, R.; Wudl, F. Highly Efficient Energy and Charge Transfer in Thin Self-Assembled Multilayered Polymer Films. *Synth. Met.* **2001**, *121*, 1367–1368.
30. Gu, Z.; Shen, Q. D.; Zhang, J.; Yang, C. Z.; Bao, Y. J. Dual Electroluminescence from a Single-Component Light-Emitting Electrochemical Cell, Based on Water-Soluble Conjugated Polymer. *J. Appl. Polym. Sci.* **2006**, *100*, 2930–2936.
31. Liu, B.; Ye, S.; Zou, Y.; Peng, B.; He, Y.; Zhou, K. A Dithienyl Benzotriazole-based Polyfluorene: Synthesis and Applications in Polymer Solar Cells and Red Light-Emitting Diodes. *Macromol. Chem. Phys.* **2011**, *212*, 1489–1496.
32. He, C.; Zhong, C.; Wu, H.; Yang, R.; Yang, W.; Huang, F.; Bazan, G. C.; Cao, Y. Origin of the Enhanced Open-Circuit Voltage in Polymer Solar Cells *via* Interfacial Modification Using Conjugated Polyelectrolytes. *J. Mater. Chem.* **2010**, *20*, 2617–2622.
33. Zhang, T.; Fan, H.; Zhou, J.; Jin, Q. Conjugated Polyelectrolyte with Pendant Carboxylate Groups: Synthesis, Photophysics, and pH Responses in the Presence of Surfactants. *J. Polym. Sci., Part A: Polym. Chem.* **2009**, *47*, 3056–3065.
34. Khan, A.; Muller, S.; Hecht, S. Practical Synthesis of an Amphiphilic, Non-ionic Poly(paraphenyleneethynylene) Derivative with a Remarkable Quantum Yield in Water. *Chem. Commun.* **2005**, 584–586.
35. Huser, T.; Yan, M.; Rothberg, L. J. Single Chain Spectroscopy of Conformational Dependence of Conjugated Polymer Photophysics. *Proc. Natl. Acad. Sci. U. S. A.* **2000**, *97*, 11187–11191.
36. Jakubiak, R.; Collison, C. J.; Wan, W. C.; Rothberg, L. J.; Hsieh, B. R. Aggregation Quenching of Luminescence in Electroluminescent Conjugated Polymers. *J. Phys. Chem. A* **1999**, *103*, 2394–2398.
37. Shin, C.-K.; Lee, H. Effect of Alkyl Side-Chain Length and Solvent on the Luminescent Characteristics of Poly(3-n-alkylthiophene). *Synth. Met.* **2004**, *140*, 177–181.
38. Bradley, D. D. C.; Grell, M.; Long, X.; Mellor, H.; Grice, A. Influence of Aggregation on the Optical Properties of a Polyfluorene. *SPIE* **1997**, *3145*, 254–259.
39. Xu, Z.; Tsai, H.; Wang, H.-L.; Cotlet, M. Solvent Polarity Effect on Chain Conformation, Film Morphology, and Optical Properties of a Water-Soluble Conjugated Polymer. *J. Phys. Chem. B* **2010**, *114*, 11746–11752.
40. Schwartz, B. J. Conjugated Polymers as Molecular Materials: How Chain Conformation and Film Morphology Influence Energy Transfer and Interchain Interactions. *Annu. Rev. Phys. Chem.* **2003**, *54*, 141–72.
41. Smith, A.; Shen, C.; Roberts, S.; Helgeson, R.; Schwartz, B. Ionic Strength and Solvent Control over the Physical Structure, Electronic Properties and Superquenching of Conjugated Polyelectrolytes. *Res. Chem. Intermed.* **2007**, *33*, 125–142.
42. Karam, P.; Ngo, A. T.; Rouiller, I.; Cosa, G. Unraveling Electronic Energy Transfer in Single Conjugated Polyelectrolytes Encapsulated in Lipid Vesicles. *Proc. Natl. Acad. Sci. U. S. A.* **2010**, *107*, 17480–17485.
43. Amrutha, S. R.; Jayakannan, M. Probing the pi-Stacking Induced Molecular Aggregation in pi-Conjugated Polymers Oligomers and Their Blends of p-Phenylenevinylenes. *J. Phys. Chem. B* **2008**, *112*, 1119–1129.
44. Chang, R.; Hsu, J. H.; Fann, W. S.; Liang, K. K.; Chiang, C. H.; Hayashi, M.; Yu, J.; Lin, S. H.; Chang, E. C.; Chuang, K. R.; Chen, S. A. Experimental and Theoretical Investigations of Absorption and Emission Spectra of the Light-Emitting Polymer MEH-PPV in Solution. *Chem. Phys. Lett.* **2000**, *317*, 142–152.
45. Chang, R.; Hsu, J. H.; Fann, W. S.; Yu, J.; Lin, S. H.; Lee, Y. Z.; Chen, S. A. Aggregated States of Luminescent Conjugated Polymers in Solutions. *Chem. Phys. Lett.* **2000**, *317*, 153–158.
46. Hsu, J. H.; Fann, W. S. Time-Resolved Fluorescence Studies of the Conjugated Polymer. *Synth. Met.* **1999**, *101*, 214–215.
47. Sherwood, G. A.; Cheng, R.; Smith, T. M.; Werner, J. H.; Shreve, A. P.; Peteanu, L. A.; Wildeman, J. Aggregation Effects on the Emission Spectra and Dynamics of Model Oligomers of MEH-PPV. *J. Phys. Chem. C* **2009**, *113*, 18851–18862.
48. Lakowicz, J. R. *Principles of Fluorescence Spectroscopy*, 2nd ed.; Kluwer Academic/Plenum Publisher: New York, 1999; pp 219−319.
49. Cadby, A. J.; Tolbert, S. H. Controlling Optical Properties and Interchain Interactions in Semiconducting Polymers by Encapsulation in Periodic Nanoporous Silicas with Different Pore Sizes. *J. Phys. Chem. B* **2005**, *109*, 17879–17886.
50. Gryczynski, Z.; Lukomska, J.; Lakowicz, J. R.; Matveeva, E. G.; Gryczynski, I. Depolarized Light Scattering from Silver Nanoparticles. *Chem. Phys. Lett.* **2006**, *421*, 189–192.
51. Michel, J. P.; Gingery, M.; Lavelle, L. Efficient Purification of Bromoviruses by Ultrafiltration. *J. Virol. Methods* **2004**, *122*, 195–198.
52. Choi, Y. G.; Rao, A. L. N. Molecular Studies on Bromovirus Capsid Protein VII. Selective Packaging of BMV RNA4 by Specific N-Terminal Arginine Residues. *Virology* **2000**, *275*, 207–217.